Photocatalytic Degradation of Malic Acid Using a Thin Coated TiO_2-Film: Insights on the Mechanism of Photocatalysis

Vanessa Rodgher, Jesus Moreira, and Hugo de Lasa
Faculty of Engineering, Chemical Reactor Engineering Centre, Western University, London, Ontario, Canada N6A 5B9

Benito Serrano
Unidad Academica de Ciencias Químicas, Programa de Ingeniería Química, Universidad Autónoma de Zacatecas, Zac., México, CP 98000

DOI 10.1002/aic.14500
Published online June 5, 2014 in Wiley Online Library (wileyonlinelibrary.com)

Decontamination of opaque fluids using photocatalysts and near Ultraviolet (UV) irradiation involves major technical challenges. This study considers a thin TiO_2 layer placed in a new Chemical Reactor Engineering Centre (CREC)-photoreactor cell. This new photoreactor cell is used for the photocatalytic degradation of malic and malonic acids, typical apple juice components. Conversion of organic species can only proceed through the "dark side" of the TiO_2 layer, which is in direct contact with the fluid. Under the selected operating conditions both external mass-transfer limitations and photolysis are found to be negligible. Macroscopic radiation balance shows that 92% of near UV radiation is absorbed by the 'back side" of the TiO_2-film. Photocatalytic degradation experiments with 10, 20, 30, and 40 ppm malic acid initial concentrations, show that malonic acid is a main intermediate. Complete malic acid conversion occurs after 5–8 h of irradiation. Kinetic modeling of malic and malonic acid photodegradation with kinetic parameter estimation is performed using both an "in series" and an "in series-parallel" reaction networks. The "in series-parallel" reaction network displays better ability for predicting CO_2 formation, showing maximum quantum yields of 14.2%. Given that in the CREC-photoreactor cell with a thin TiO_2-film, photocatalysis can only proceed via the transfer of mobile "h^+" sites from the irradiated side to the "dark side', this study demonstrates the significance of this step on the overall photocatalysis mechanism. © 2014 American Institute of Chemical Engineers *AIChE J*, 60: 3286–3299, 2014
Keywords: photocatalysis, TiO_2-film-catalyst, back-face irradiation, malic acid, malonic acid, kinetic modeling, quantum yield, apple juice, sensory attributes

Introduction

Photocatalysis, using TiO_2 as a catalyst, is a well-known process for the degradation of pollutants in water treatment. A photocatalytic reaction starts when the semiconductor catalyst is irradiated by a light source with a wavelength range smaller than 400 nm (optimum 365 nm) and with a higher energy than the energy of the catalyst's band gap.[1,2] The light is absorbed by the catalyst creating electron-hole pairs. The holes react with water producing OH radicals and the electrons react with the dissolved O_2 producing oxidant species. Both holes and electrons react by degrading the organic molecules present in the solution into CO_2 and H_2O.

Photocatalytic reactions can be performed with the catalyst in suspension or immobilized on a thin film or a mesh. Although a photocatalyst in suspension is the most general form used for the photocatalytic process, it appears to present some limitations. The most significant one is the filtration requirement to remove the catalyst at the end of the reaction. Conversely, the use of photocatalyst films has the benefit of not requiring the water effluent to be filtered, introducing significant cost, and time savings in industrial scale processes.

Many semiconductors have been used in photocatalytic processes. In this respect, TiO_2 is the measuring "stick" against which emerging materials are compared. There are two types of TiO_2 catalysts available: anatase and rutile. Degussa P25 has been extensively used for photocatalytic reactions as it is composed of a mixture of anatase and rutile. This catalyst presents a band gap energy of 3.2 eV. Thus, any photon with a wavelength smaller than 388 nm is capable of exciting the Degussa P25 promoting photocatalytic degradation.[2]

Charge carrier mobility in semiconductor films was performed by a number of authors.[3–7] In particular, Enright and Fitzmaurice[3] studied nanocrystalline TiO_2 (anatase) films at 300 K, reporting an electron mobility and an electron diffusivity of 0.4×10^{-4} $m^2/(V\ s)$ and 1×10^{-6} m^2/s respectively. Conversely, the same authors reported an electron hole mobility and a diffusivity of 1.6×10^{-3} $m^2/(V\ s)$ and 4×10^{-5} m^2/s. On the basis of this data, these authors calculated the time required for a carrier to transit from the

Correspondence concerning this article should be addressed to H. de Lasa at hdelasa@eng.uwo.ca.

interior of the TiO_2 crystallite to the surface. It was observed that an electron in a 8 nm (4 nm radius) particle displays a transit time of 2 ps. Furthermore, the transit times for electron holes can be assessed at 0.4 ps. Thus, expected electron and hole velocity is 2000 and 10,000 m/s, respectively.

Ultraviolet (UV)-light treatment is a well-known technique used for the disinfection of fruit juice due to its capacity to attain the 5-log CFU/mL microorganism reduction. This is accomplished without producing significant changes in the sensorial and physical–chemical characteristics of the juice.[8] According to Hanes et al.[8] a semitransparent juice, such as apple juice, absorbs UV-light at 253.7 nm and only a small amount of the light emitted reaches both organic molecules and microorganisms.[9]

Due to the low penetration of light in these fluids, UV systems are usually designed with the fluid injected as a thin film.[8,10,11] It was proven by Duffy et al.[10] that the effectiveness of the 5-log CFU/mL reduction of *Escherichia coli* using a thin film system with 10-UV lamps. In the light of these findings, new methods for the degradation of microorganisms in fruit juice are needed. One possible alternative could be the use of advanced oxidation methods for juice decontamination. These methods have been very successful for the degradation of organic pollutants in water and appear to be a very good alternative for organic acids degradation in opaque fluids.

Different methods for the preparation of photocatalyst films have been developed on surfaces such as glass, quartz, stainless steel,[12] and optical fibers.[13] Their preparation involves different processes including the immersion of a support in titanium mixtures, drying, and calcination, among others.[1,13–17] These methods are time consuming and costly in terms of materials and equipment. Thus, new techniques for photocatalyst immobilization at a low cost may be of great importance for the photodegradation of organic acids in water and for their subsequent application in opaque fluids.

Although there are many organic molecules in common between fruit juice media and wastewater, differing techniques have been used for their decontamination. Opaque fluids such as fruit juice have as main components organic acids. These chemical species are classified as weak acids and are frequently formed as intermediates from the incomplete degradation of organic species.[18] Although organic acids do not appear to be hazardous compounds, their study is extremely important to understand how degradation methods influence the main chemical composition of opaque fluids media such as apple juice.[19]

The photocatalytic degradation of microbial microorganisms such as *E. coli* in water media using TiO_2, both in suspension and immobilized, has been reported by diverse authors.[20–22] These studies show good promise for photocatalysis applications with a 5-log CFU/mL pathogen reduction reached in water media. Moreover, the use of photocatalysis for organic acid photodegradation in water using suspended and immobilized TiO_2 has also been reported more recently.[2,23,24] In the case of opaque fluids, photocatalyst films appear as an alternative to overcome the high absorption of irradiation by these fluids. In this respect, one can envision immobilized TiO_2 on various thin film substrates. This is required to combine good microbial microorganism inactivation and very limited photodegradation of malic acid and its intermediates, preserving sensorial properties of opaque fluids.

The present investigation contributes with a comprehensive study of the photocatalytic degradation of selected organic acids, major apple juice components. The chosen approach is to use an immobilized photocatalyst thin film, placing it under near UV-light source irradiation. The photocatalyst layer is prepared by coating a square quartz window using a UV-transparent/waterproof glue and a 1.5 wt % TiO_2 solution in water. The apparatus is completed with a near UV-light source strategically located to secure a high degree of irradiation of the thin film. The Chemical Reactor Engineering Centre (CREC)-Photo reactor cell is equipped with the required spectrophotoradiometer to perform measurements which provide the data for macroscopic radiation balances. Using this setup, the TiO_2 layer side in direct contact with the fluid is not directly irradiated. Therefore, only mobile "h^+" holes are able to contribute to photoconversion. Thus, in addition to establishing a valuable approach to describe malic acid and malonic acid degradation using TiO_2 thin films under near UV-light, our results allowed us to demonstrate the unique role of mobile h^+ charges on TiO_2-films. As well and from a practical standpoint, this study establishes the required irradiation times for microbial decontamination under conditions, where key chemical species responsible for the sensorial properties of the fruit juice are preserved.

Experimental Methods

TiO_2-film 1.5 wt % preparation

To immobilize the TiO_2 catalyst, a thin layer containing a homogeneous coverage of TiO_2 catalyst was prepared. The support chosen for the TiO_2-film was quartz, which appears to promote a better TiO_2 activity when compared to other supports.[1,12] In the initial step, the quartz surface with a thickness of 1.62 mm was washed with water, a MICRO laboratory Cleaner (Cole-Parmer Instrument Company), and 95% ethyl alcohol (Commercial Alcohols).

Since other more expensive methods have been proposed in the technical literature,[13–17] a new method for TiO_2-film coating was developed. The proposed method uses a UV-transparent/waterproof glue and a TiO_2 Degussa P25 (Evonik Degussa Corporation Lot 4168012498). The glue used on the quartz surface was the UV-transparent/waterproof glue LOCTITE® 3321™.

The steps to prepare the TiO_2-film are as follows:

a. Spread Loctite Glue homogeneously over the quartz surface;
b. Let the glue dry partially for 24 h;
c. Prepare a TiO_2 Degussa P25 1.5 wt % solution;
d. Spread the catalyst solution over the glue (repeat it three times);
e. Cure the layer for 1 h with UV-visible light (radiation at 254 nm).

Figure 1 describes the batch CREC-photoreactor cell bottom surface coated with a TiO2-film using the method developed in this study. Good uniformity and reproducibility of the TiO2-film was confirmed with SEM-EDX with TiO2 covering 70–80% of the exposed area as described in Absorption spectra in water and opaque fluids section of this article.

The batch CREC-photoreactor cell with the bottom surface coated with the TiO2-film was kept in storage with a minimum exposure to UV-visible light. A cooler system

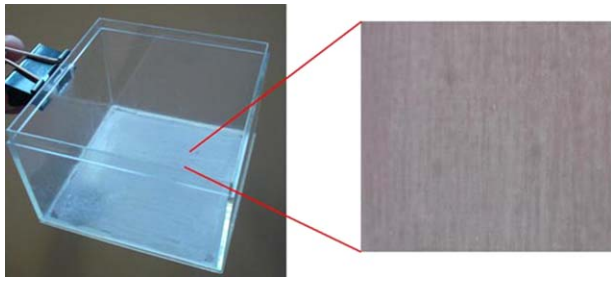

Figure 1. Batch photoreactor cell of this study with one side coated with the TiO_2-film 1.5 wt % solution.

[Color figure can be viewed in the online issue, which is available at wileyonlinelibrary.com.]

composed of a cooling tank, an outer box, and a pump, were the accessories that completed the photoreactor cell setup. This allowed maintaining the cell temperature in the $10 \pm 5°C$ range during the entire photodegradation experiment. Precautions were taken following indications according to the technical data sheet of the LOCTITE® 3321™, to keep the physical–chemical properties of the glue.

Reactants

The following reactants were used as received without further purification: malic acid (Sigma-Aldrich, Lot 058K0018V), malonic acid 99% (Sigma-Aldrich, Batch 04008PC), phosphoric acid 85% (Fluka Analytical, Lot BCBD9465). Samples of 10, 20, 30, and 40 ppm of malic acid and malonic acid were prepared in deionized water to perform the photodegradation experiments. The detection of malic and malonic acid were performed in a HPLC Shimadzu Prominence LC 20AB, with a column oven CTO-0AC, an Autosampler SIL-20AC.HT and a diode array detector SPD-M20A. The column utilized for the organic acids measurements was an Ion Exchange Supelcogel C-610H column 30 cm × 7.8 mm ID (59320-U). The mobile phase used was phosphoric acid H_3PO_4 0.1% (v/v) at a flow rate of 0.5 mL/min. The temperature of the column oven was controlled to be in the range of $30 \pm 5°C$, the UV detection wavelength was set to 210 nm and an injection volume of 50 μL for malic and malonic acid solution was used. All the samples analyzed in the HPLC were previously filtered using a PTFE Mandel 0.2 μm Filter.

CREC photoreactor cell setup

A new CREC-photoreactor cell was developed at the CREC. The main goal for the photoreactor cell was to establish a setup with an immobilized TiO_2 catalyst layer. In this new setup, an external UV-lamp was placed facing the interface support-TiO_2-film. In this way, the TiO_2-film received irradiation before photons could reach the opaque fluid. In order for this reaction to proceed, generated electron-hole pairs had to migrate to the other face of the quartz slide (dark side), where the photocatalyst was in direct contact with the fluid.

This CREC-Photo cell allows to place the spectroradiometer head at strategic locations in the Photo-CREC cell such as: (a) at the film surface allowing irradiated measurements of irradiated photons reaching the TiO_2-film (P_i), (b) at the back of the TiO_2-film permitting quantification of photons transmitted through the TiO_2-film (P_t), and (c) at the front of the TiO_2-film allowing measurement of the backscattered irradiation photons (P_{bs}).

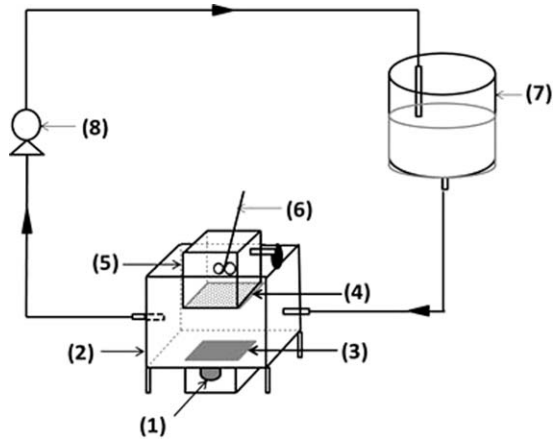

Figure 2. The CREC-photoreactor cell setup used in the photocatalytic degradation of malic and malonic acids.

Figure 2 reports the CREC-photoreactor cell setup used for the photocatalytic degradation of malic and malonic acid. This photoreactor cell consists of: (1) an external near UV-light lamp, (2) an outer box to keep the temperature in the range of $10 \pm 5°C$, (3) a quartz window at the bottom of the outer box, (4) a TiO_2-film 1.5 wt % coated on a quartz surface, (5) a batch photoreactor, (6) a stirrer, (7) a cooler tank, and (8) a centrifugal pump. The CREC-photoreactor cell setup, as well as the properties of the near UV-lamp, reported in Figure 2 are described Table 1.

Photodegradation experiments

Before each photodegradation experiment, the CREC photoreactor cell was cleaned carefully with fresh water and rinsed with distilled water to eliminate any chemical species from previous runs. Solutions of malic and malonic acid at different concentrations (10, 20, 30, and 40 ppm) were prepared from a 1000 ppm stock solution using deionized water.

In addition, prior to starting the experiments, an initial sample was taken and analyzed to determine the initial organic acid concentration. Following this, the reactor setup

Table 1. Characteristics of the CREC-Photoreactor Cell Setup

Component	Parameter	Measurement
Batch reactor	length	9 cm
	width	9 cm
	height	9 cm
	volume	200 mL
	quartz thickness	0.16 cm
Outer Box	length	11.3 cm
	width	11.3 cm
	height	11.3 cm
	height legs	4.5 cm
	volume	5 L
Cooler Tank Stirrer	speed	250 RPM
UV-Lamp	length	41.3 cm
(UVP-XX-15BLB)	radius	1.33 cm
	Input power	15 W
	Output power	4 W
	Emission range	320–420 nm
	Emission rate	1.1910×10^{-5} Einstein.s^{-1}

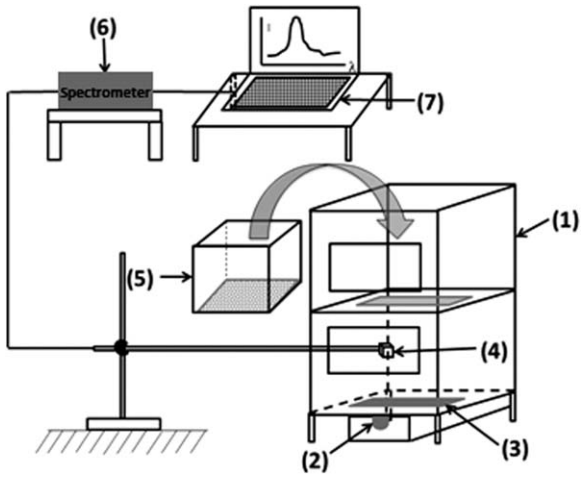

Figure 3. Schematic representation of the radiation measurements of the CREC-photoreactor cell with the TiO_2-film.

was run for 30 min in the dark to reach adsorption equilibrium on the TiO_2 layer surface. At this point, a second sample was taken. Once adsorption equilibrium was reached, the lamp was turned on and the photocatalytic degradation was initiated.

Once the run started, samples were taken every hour for 15 h to analyze the change in malic and malonic acid concentrations during the photocatalytic conversion. All the experiments were performed at set operational parameters, such as: (a) light intensity emission, (b) catalyst loading, (c) initial pH (4.0 ± 0.1), and (d) temperature (15 ± 3°C). All the experimental runs were repeated three times to ensure experimental reproducibility.

Radiation measurements

To determine the rate of photons absorbed by the TiO_2-film, radiation measurements of the catalyst layer were performed. A radiation box with the same dimensions of the photoreactor cell was used. Measurements were performed using a light detector probe which was connected to a spectrometer and a SpectraWiz software. The radiation measurements setup (refer to Figure 3) was composed of: (1) a radiation box, (2) a near UV-lamp, (3) a quartz window, (4) a light detector probe, (5) a photo batch reactor, (6) a StellarNet EPP2000C-25 LT16 Spectrometer, and (7) the SpectraWiz Software. In this setup, the light was placed at the bottom of the radiation box. Lamp asymmetrical positioning is described in Figure 4. A description of lamp asymmetric positioning is important to explain the various types of radiation such as emitted, backscattered, transmitted, and reflected radiations.

Results and Discussion

Absorption spectra in water and opaque fluids

Preliminary experiments were performed to assess the photoconversion of organic acids in opaque fluids using a commercial apple juice (Allens' concentrate). The apple juice was tested using the Photo-CREC Water-II. This reactor unit has been previously used for photodegradation of organic compounds in water treatment showing its high quantum efficiency.[2,25–29] However, Photo-CREC Water II reactor is not adequate for opaque fluids. Under these conditions, photocatalytic reactors with immobilized TiO2 on films as in the proposed CREC-Photo Cell are more adequate.

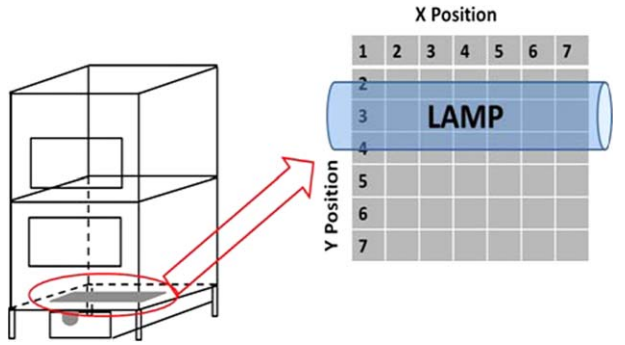

Figure 4. Description of the 49 positions to establish the nonsymmetrical radiation profile.

[Color figure can be viewed in the online issue, which is available at wileyonlinelibrary.com.]

Figures 5 and 6 report the spectra for apple juice and water. The light transmission spectrum in apple juice shows a light intensity distribution along a wavelength range of 320–420 nm, with a 0.6 $\mu W/cm^2$ at 380 nm maximum intensity. However, the maximum intensity for the water spectra is 58 $\mu W/cm^2$ at 370 nm or 100 times larger than in apple juice. Thus, in apple juice, there is a very significant irradiation absorption limiting transmittance in the near-wall regions. As a result, transmittance is significantly reduced and the amount of irradiation reaching the photocatalyst decreases considerably.

One can, thus, conclude that the use of suspended TiO_2 in opaque fluids becomes impractical because the opacity of the fluid largely prevents light from reaching the photocatalyst. This reduces the formation of electron-hole pairs, which are responsible for the organic species photoconversion.

Regarding irradiation transmission in photocatalytic reactors, Figures 7a, b illustrate two different modes of electron hole formation: (a) Figure 7a shows the "directly" irradiated

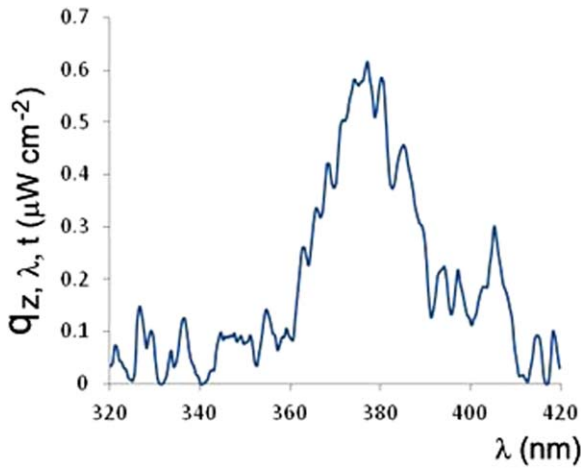

Figure 5. Transmission spectra for commercial Allens apple juice at position 4 (Brix: 11.90 ± 0.1, pH: 3.10 ± 0.05, conc. of malic acid: 3 ± 0.1 g/L).

[Color figure can be viewed in the online issue, which is available at wileyonlinelibrary.com.]

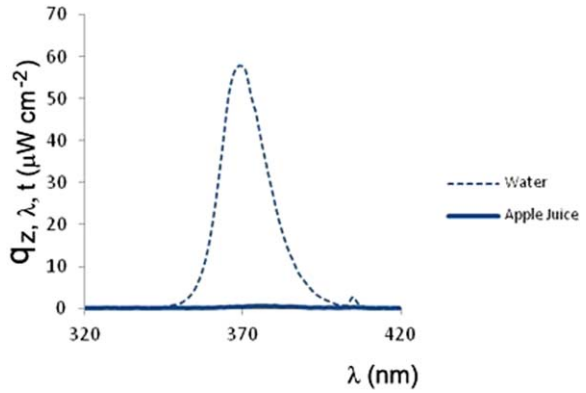

Figure 6. Apple juice transmission spectra and water transmission spectra.

[Color figure can be viewed in the online issue, which is available at wileyonlinelibrary.com.]

suspended photocatalyst as in PhotoCREC-Water II and (b) Figure 7b describes the TiO_2-film with "non-directly" irradiated photocatalyst surfaces promoting photoconversion as in the Photo-CREC cell. It is hypothesized that this mechanism is important in the Photo-CREC Cell due to the mobility of the "h^+" electron holes. This is accomplished thanks to the special approach for film preparation securing TiO_2 particles being in one hand in direct contact with the fluid and on the other, being irradiated from the back face (refer to Figure 7b).

Thus, "h^+" and "e" charge mobility leads to the formation of OH• groups in the particle hemisphere in direct contact with the water solution. This may potentially occur with a 2 photons forming 3 OH• groups, as postulated by our research group.[30,31]

Figure 8 displays SEM results showing that TiO_2 coated particles form a wavy layer. Figure 9 reports an EDX (Energy Dispersive X-Ray) analysis of specific regions of

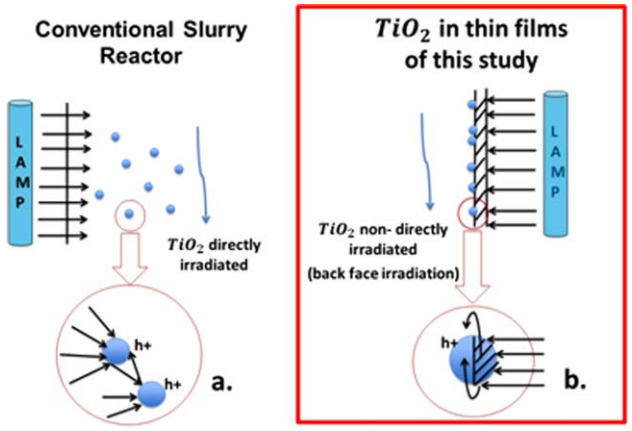

Figure 7. Irradiation paths showing the formation of electron holes (h^+) on (a) the outer surface of suspended and "directly irradiated" TiO_2 particles as in a photo CREC water II reactor and (b) the outer surface of "non-directly" irradiated TiO_2 with h^+" mobile electron holes promoting photoconversion as in a CREC-photoreactor cell.

[Color figure can be viewed in the online issue, which is available at wileyonlinelibrary.com.]

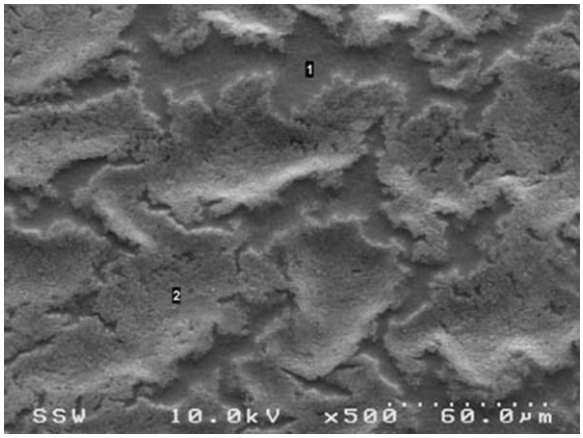

Figure 8. SEM of TiO_2 Film (500×): Region 1–surface with near absence of TiO_2 photocatalyst coverage; Region 2–surface with significant coverage of TiO_2 photocatalyst.

the film. Region 1 shows 10 microns × 60 micron zones where there is a near absence of TiO_2. Region 2 (refer to Figure 8) describes identifiable 30micron × 60 micron TiO_2 covered areas with likely a 1 micron characteristic SEM-EDX microanalysis depth. This characteristic wavy thin film with two different levels of coverage was assumed to be the result of glue properties and can be traced to the curing step, where the TiO_2-film was subjected to 1 h of intense irradiation at a wavelength of 254 nm. On the assumption that TiO_2 particles such as the ones in "2" were directly in contact with water, it was estimated 73.7% of the film containing TiO_2 was in direct contact with water. On this basis, an estimated surface concentration of TiO_2 on the film was estimated at 2.1×10^{-4} g/cm^2.

Photolysis and photocatalytic degradation of malic acid using TiO_2-films and in suspension

The photocatalytic degradation of malic acid and the formation of malonic acid were measured using the HPLC method described in the experimental section. Malonic acid appeared as the main intermediate species formed during malic acid photoconversion. This is in agreement with other research studies published in the literature.[13,18,32]

Figure 10 reports a typical concentration profile for malic acid degradation and malonic acid formation as a function of time using a TiO_2-supported photocatalyst layer. It can be observed that the photoconversion of malic acid is achieved after 6 h of thin film irradiation. This is about the time when the malonic acid concentration appears to display a maximum value.

Figure 11 reports malic acid photoconversion for four initial malic acid concentrations (10 to 40 ppm). All experiments were repeated three times to ensure reproducibility. One can observe complete malic acid photoconversion in 5 to 8 h. Moreover, Figure 12 also shows malonic acid concentration changes, with malonic acid increasing first and then, later decreasing. Thus, malonic acid was consistently observed as an intermediate species in malic acid photoconversion.

According to the technical literature,[33,34] a potential disadvantage of thin layers of immobilized photocatalysts is their limited potential irradiation and restricted external mass-

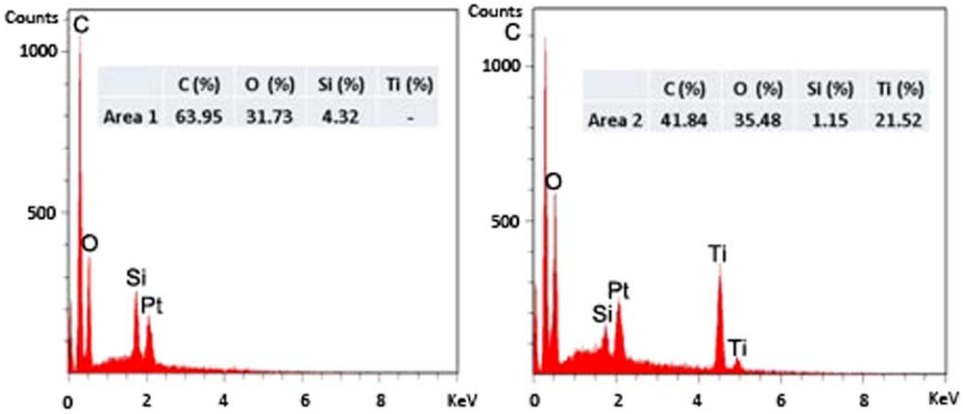

Figure 9. EDX analysis of TiO_2 Film–Regions 1 and 2 from Figure 88.

[Color figure can be viewed in the online issue, which is available at wileyonlinelibrary.com.]

transfer rate. It is estimated that a 5 μm TiO_2-film allows adequate irradiation.[34]

Moreover and to clarify the potential effect of a TiO_2-film external mass transfer on malic acid photodegradation, photocatalytic runs were performed using two different mixing speeds. Figure 13 reports the photodegradation using 40 ppm of initial malic acid at 125 and 250 rpm stirrer speeds. One can see that there is no observable difference in photoconversion rates when the mixing speed is changed from 125 to 250 rpm. One can conclude that the relatively high fluid circulation in the near thin film region, estimated at 24 and 47 cm/s, respectively, promotes high mixing and negligible external mass transfer on the overall photoconversion rate.

In addition, one can provide an estimate of the external mass transfer influence in the near photocatalyst layer region as follows: (a) by considering a Sherwood number of 2 (Sherwood number at stagnant conditions) and (b) by performing a malic acid mass balance between the photocatalyst film and the solution near the thin film region. This allows a comparison of the external mass-transfer coefficient (k_m) and the intrinsic kinetic constant (k_i), showing a k_m of 1.604×10^{-3} m/s which is about 1000 times higher than k_i ($k_i = 4.45 \times 10^{-6}$ m/s). This confirms that the external transfer mass influence in the near thin film region can be disregarded in malic acid photoconversion kinetic modeling.[19]

When organic compounds are irradiated by a near-UV source, they can be degraded via photolysis.[35–37] The influence of photolysis on the photodegradation has been studied using both water as well as opaque fluids. UV-light treatment has been utilized for opaque fluid disinfection such as for fruit juice. UV-light treatment has the ability to keep the taste and odor characteristics of fruit juices. UV-light treatment has also been approved since the year 2000 by the American Food and Drug Administration (US FDA, 21CFR120) as a pathogen reducer in juice.

Photolysis can affect photocatalytic conversion. Thus, for proper kinetic modeling, one needs to assess the influence of photolysis in the case of TiO_2-films used in the CREC-photoreactor cell. For instance, in the case of malic acid, one should compare its degradation profile with and without TiO_2-films. Using this data, one can accurately account for the role of photocatalytic malic acid photoconversion discounting the photolysis effect.

Figure 14 reports malic acid concentration changes when a 20 ppm solution of malic acid was irradiated using a near-UV lamp in the CREC-Photo cell. Two cases with and without the TiO_2-film mounted in the photoreactor cell unit, were considered. According to these results, almost complete photocatalytic degradation of 20 ppm of malic acid is achieved when using a TiO_2-thin film in 6 h, with only 0.8 ppm of malic acid remaining. Conversely, malic acid

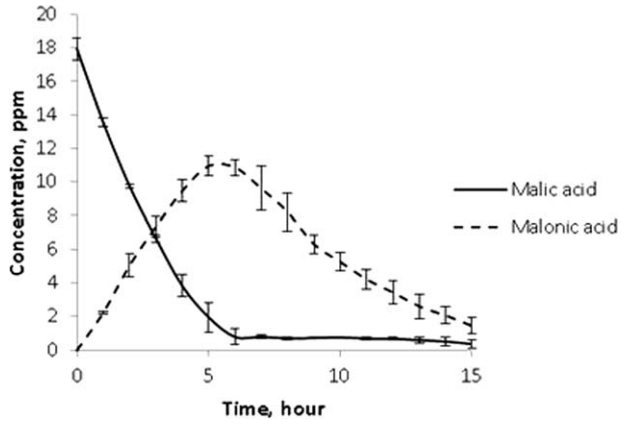

Figure 10. Photodegradation profile of malic acid using a TiO_2 film and a near UV-light.

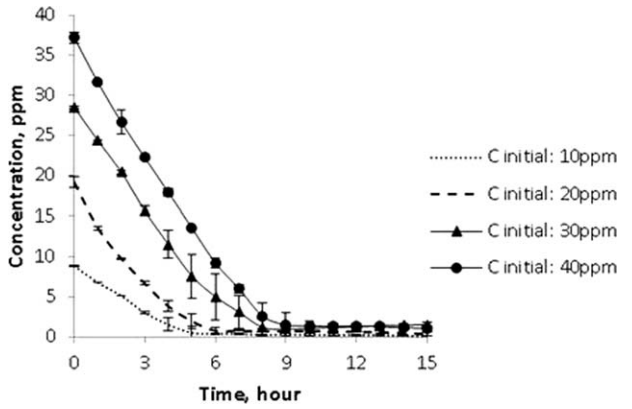

Figure 11. Malic acid photodegradation profile for different initial concentrations: 10, 20, 30, and 40 ppm.

Reported experimental data are for three repeat experiments.

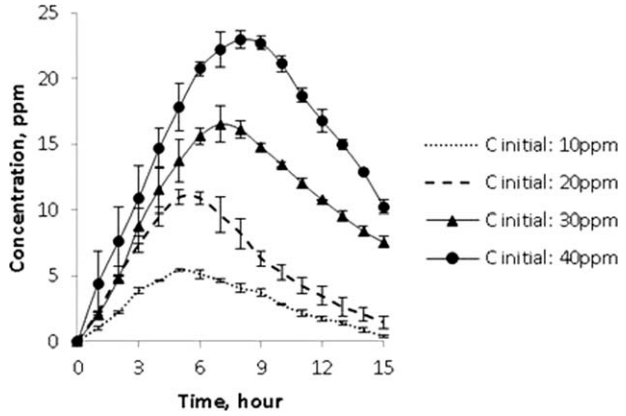

Figure 12. Malonic acid evolution during photodegradation initial malic acid concentrations: 10, 20, 30, and 40 ppm.

concentration decreased by 24% during the same irradiation period when no TiO_2-film was used in the CREC-Photorecator cell.

However, to properly assess the role of photolysis, one needs to carefully consider all factors involved in the CREC-photoreactor cell unit. The photolysis rate depends on both the malic acid concentration and irradiation intensity (I) reaching the malic acid solution (transmitted radiation) as shown in the following equation

$$\frac{dC_i}{dt} = -(k'_{\text{photolysis}} I)C \tag{1}$$

where C_i represents the species concentration at any time during the photoconversion, I is the transmitted irradiation in the CREC-photoreactor cell, t stands for the irradiation time, and $k_{\text{photolysis}}$ denotes the photolysis reaction rate constant.

As will be described later in this article, I, the transmitted irradiation in the CREC-photo reactor cell amounts to 4% of the total radiation reaching the TiO_2-film (I'). Thus, Eq. 1 can be rewritten as follows

$$\frac{dC_i}{dt} = -(k'_{\text{photolysis}} 0.04 I')C \tag{2}$$

Equation 2 can be integrated over the irradiation time and the resulting malic acid concentration changes can be compared with the experimentally values observed. Given Eq. 2 and the experimental data for the photolysis of 10, 20, and 30 ppm malic acid and malonic acid initial concentrations, the following kinetic constants as reported in Table 2 were obtained.

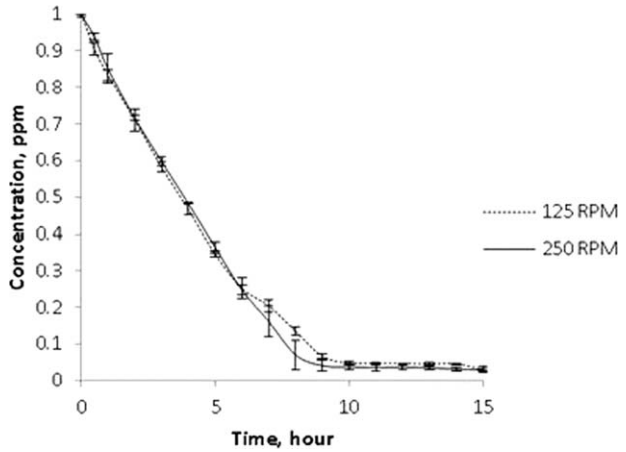

Figure 13. Malic acid concentration photodegradation experiment using a TiO_2 film at two different mixing speeds: 125 and 250 rpm.

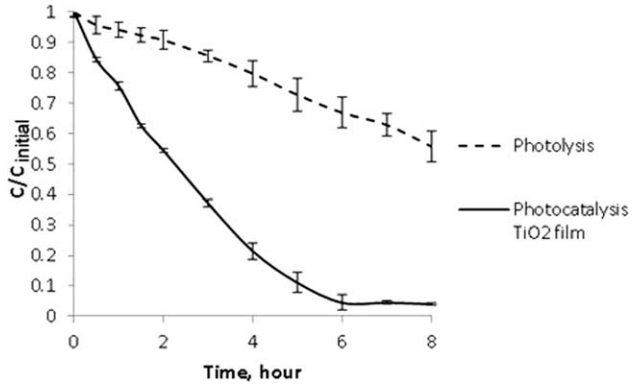

Figure 14. Malic acid concentration changes at 20 ppm of initial malic acid concentration using a near UV irradiation lamp.

Broken line: Photoconversion in the CREC-photoreactor cell due to photolysis only, (b) Photoconversion in CREC-photoreactor cell using a TiO_2 thin film.

Using this approach, one can show that photolysis contributes to 1% malic acid concentration change only, as shown in Figure 15. Thus, this very small concentration change can be considered negligible and photolysis can be disregarded when using an irradiated TiO_2-film in a CREC-photoreactor cell unit.

Contrary to photocatalysts in suspension, immobilized photocatalysts do not require a filtration step, allowing a reduction of both cost and time in an industrial scale process. This is particularly valuable in the case of the preconditioning of fruit juice for human consumption. In any event and to have a basis for comparison, malic acid photoconversion using TiO_2 1.5 wt % films and TiO_2 in suspension were performed using 20 ppm malic acid initial concentration. Different loadings of TiO_2 were used (0.01, 0.05, 0.10, 0.15, 0.20, and 0.30 g L^{-1}). Figure 16 shows that malic acid photodegradation increases with the photocatalyst loading. Figure 17 shows that photocatalyst loadings higher than up to 0.2 g L^{-1} or extra photocatalyst did not change the photoconversion rates significantly.

TiO_2 in suspension can be used to perform organic species photocatalytic degradation in water, as reported in a number of studies by our research group.[27–29,38] The Photo-CREC Water II's high efficiency for the complete mineralization of organic compounds in water forming CO_2 and H_2O has been demonstrated.[2]

However, even though malic acid photodegradation in the Photo-CREC Water II is expected to lead to higher photoconversion rates when using fine TiO_2 particles (20–60 nm), the application of TiO_2 in suspension is limited to translucent fluids and cannot be extended to opaque fluids. In

Table 2. Kinetic Constants for the Photolysis of Malic and Malonic Acid

Parameter	Compound	Value	95% CI
$k_{\text{photolysis}}(\text{min}^{-1})$	Malic Acid	7.727×10^{-4}	2.391×10^{-5}
$k_{\text{photolysis}}(\text{min}^{-1})$	Malonic Acid	3.984×10^{-4}	1.946×10^{-5}

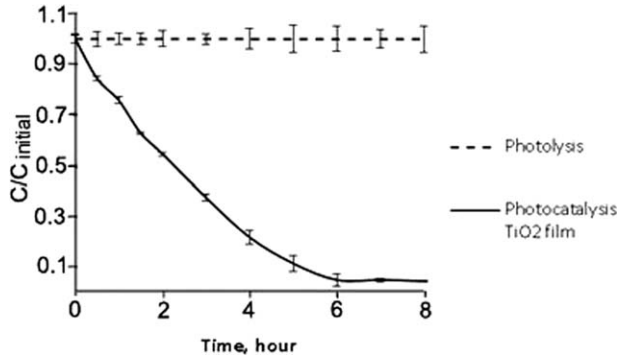

Figure 15. Degradation profile for photolysis and photocatalytic conversion by using a TiO_2 film.

Malic acid: 20 ppm. Broken like corresponds to the calculated malic acid changes using a photolysis kinetics as per Eq. 2 and a 4% irradiation transmitted through the film.

addition, TiO_2-films have to be specially tailored for organic species photocatalytic degradation in opaque fluids. These TiO_2 films must have an active nonirradiated dark side as described in Figure 7b. These types of TiO_2 films may also offer an effective approach that sheds light into the photocatalytic mechanism. This is due to the fact that photocatalytic activity can only result from the mobility of h^+ electron holes.

Irradiation measurements

Irradiation analysis includes determining the following: (1) the radiation being emitted by the lamp (P_l), (2) the radiation reflected (back-scattered) by the catalyst film (P_{bs}), and (3) the radiation transmitted through the film (P_t). Salaices-Arredondo[25] used a macroscopic balance approach performed in an annular photoreactor with the photocatalyst in suspension. A similar methodology can be used in the CREC-photoreactor cell to determine the radiation absorbed by the catalyst (P_a). P_a is of utmost importance for calculating reactor efficiencies in the photodegradation of organic compounds. Several authors have discussed radiation measurements in photoreactors with TiO_2 in suspension.[39,40] However, very few researchers have studied the radiation using photocatalyst catalyst films.

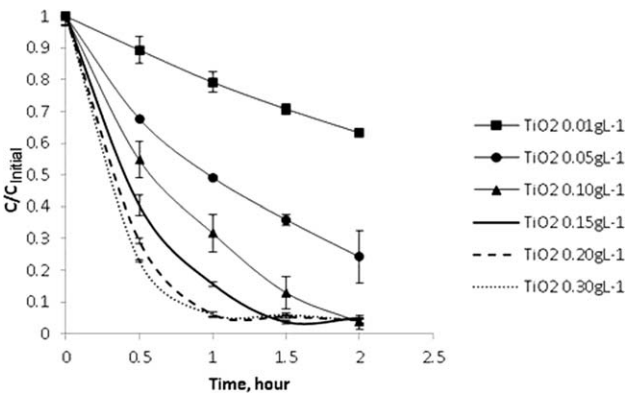

Figure 16. A 20 ppm malic acid photodegradation profile for different TiO_2 concentrations in suspension: 0.01, 0.05, 0.10, 0.15, 0.20, and 0.30 g L^{-1}.

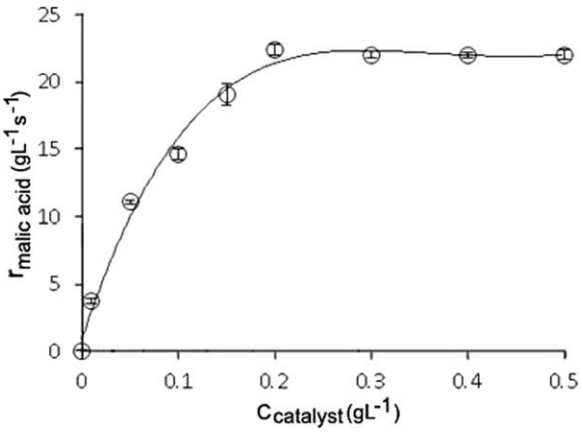

Figure 17. Rate equation for malic acid degradation ($r_{malic\ acid}$) using different TiO_2 concentrations in suspension (0.01 to 0.5 g L^{-1}).

Initial concentration of malic acid: 20 ppm.

In the CREC-photoreactor cell, the lamp is placed below a quartz box (refer to Figures 3 and 4) The selected positioning is well inside the lamp's constant radiation emission zone. This placing of the lamp minimizes losses of light that occur at the edges of the lamp. Figure 18 reports the spectrum for the lamp used in this study. This spectrum was measured using a spectroradiometer 4 cm away from the center of the lamp and 22 cm from its edge.

In all the photodegradation experiments developed in this study, UV-lamps had less than 1000 h of use. Thus, lamp emission decay could be considered negligible, this has already been reported somewhere else.[27,41]

A macroscopic radiation balance allows the calculation of the P_a, which is the rate of radiation absorbed by the TiO_2 film. This is done by using the results of: (a) the radiation emitted by the lamp, (b) the radiation reflected by the catalyst layer (backscattered), and (c) the radiation transmitted through the catalyst film using the expression shown in Eq. 3 [2]

$$P_a(t) = P_1(t) - P_{bs}(t) - P_t(t) \tag{3}$$

where $P_a(t)$ is the rate of absorption of photons, $P_{bs}(t)$ is the rate of backscattered photons exiting the system, $P_t(t)$ is the

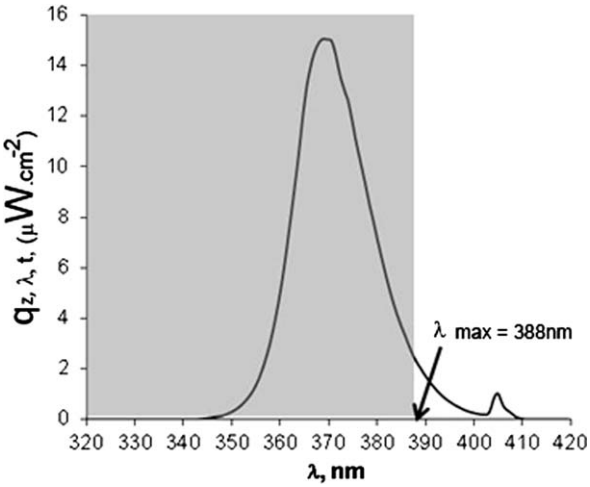

Figure 18. Emission spectrum for black UV lamp.

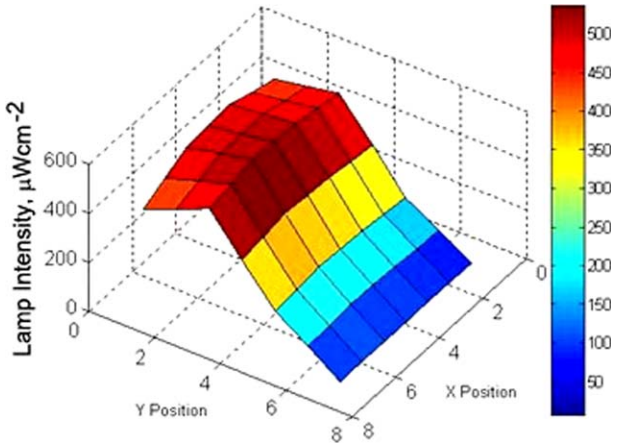

Figure 19. $P_l(t)$ spectrum along the 49 positions as described in Figure 44.

[Color figure can be viewed in the online issue, which is available at wileyonlinelibrary.com.]

rate of transmission of photons, and $P_l(t)$ is the rate of emission of photons by the lamp, all in Einstein.s^{-1} units.

P_1 was calculated by using the following expression[2]

$$P_1(t)=\frac{\bar{\lambda}}{h\cdot c}\int_{\lambda_1}^{\lambda_2}\int_0^{\infty}\int_0^{2\pi} q_{\theta,z,\lambda,t}\cdot r\cdot d\theta dz d\lambda \qquad (4)$$

where h represents the Planck's constant (6.626×10^{-34} J s), c denotes the speed of light (2.998×10^{8} m s^{-1}), $q_{\theta,z,\lambda,t}$ stands for the radiative flux (µW cm^{-2}), r represents the radial coordinate (m), z denotes the axial coordinate (m) and $\bar{\lambda}$ stands the average emission wavelength (nm).

As mentioned before, in the setup of this study, an external near UV-lamp irradiates the batch through one radial side only. Thus, considering the symmetrical angular emission of the BL-lamp, Eq. 4 can be simplified as follows

$$P_1(t)=\frac{\bar{\lambda}}{h\cdot c}\int_{\lambda_1}^{\lambda_2}\int_0^{L} q_{z,\lambda,t}\cdot r\cdot dz d\lambda \qquad (5)$$

where ($\bar{\lambda}$) is the average calculated wavelength in the 320–388 nm range, when using the weighted mean method.

The near UV lamp intensity (µW cm^{-2}) was measured between $\lambda_1=320$ nm and $\lambda_2=420$ nm along the 81 cm^2 area, which represents the quartz surface area covered by the TiO_2-film. Radiation measurements were performed in 49 different positions, divided equally into seven parts in each X and Y direction. In this way, it was possible to develop a precise radiation spectrum taking into consideration the asymmetrical position of the lamp relative to the photocatalytic reactor. One should notice that in the experimental setup, the lamp was placed between Y positions 2 and 4 along the X axis.[19]

Figure 19 reports the 3-D spectra of lamp intensity emitted by the lamp. This plot shows an asymmetrical radiation profile, with higher values of intensity emitted in the Y position 3, between the X positions 3 and 5.

Regarding the P_a, P_l, P_{bs}, and P_t parameters involved in the radiation macroscopic balance, they were calculated by performing the integration of radiation measured in the 49 positions. This will be discussed in the next section. An estimated $P_l(t)$ value was established with 49 radiometric measurements. The resulting $P_l(t)$ obtained was 4.04×10^{16} photons/s. The calculation of $P_a(t)$ was performed using Eq. 3 and the $P_{bs}(t)$ and $P_t(t)$ were obtained experimentally. These results are reported in Table 3. It can be concluded that a significant amount of the near UV radiation is absorbed by the TiO_2 film (92%). Thus, it can be observed that the radiation absorption results reported in this study are close in magnitude to the values reported for TiO_2-coated optical fibers.

Table 3. P_l (t), P_{bs} (t), P_t (t), and P_a (t) Calculated for the TiO_2-Film

	Rate of Photon (Photons/s)	Irradiation (%)
Emitted, P_l (t)	4.41×10^{16}	100
Back Scattered, P_{bs} (t)	1.95×10^{15}	4
Transmitted, P_t (t)	1.75×10^{15}	4
Absorbed, P_a (t)	4.04×10^{16}	92

Kinetic modeling of malic acid photocatalytic degradation

The Langmuir–Hinshelwood (L–H) approach provides a well-known model to describe the catalytic conversion of chemical species involving adsorption at equilibrium. Several authors have used L–H to represent the heterogeneous photoconversion kinetics of organic species photodegradation onof(check) TiO_2 catalysts.[12,23,28,29,32,38,41–43] L–H has the advantage of considering not only the model compounds but also the intermediates formed during the photocatalytic conversion. In our study, only the main intermediate, malonic acid, was identified and considered in the modeling.

In modeling the heterogeneous kinetics of malic photodegradation using a thin-TiO_2 catalyst film developed in this study, two reaction mechanisms can be proposed. Both models consider malonic acid as an intermediate species resulting from malic acid photodegradation. The first model is an "in series" reaction network (RN1), whereas the second model assumes an "in series-parallel" reaction network (RN2). These models are shown in Figures 20 and 21, respectively.

The kinetic modelling for the two reaction mechanisms requires that the following assumptions be adequate:

a. Malic and malonic acids must adsorb on the TiO_2 film surface where the photocatalytic reactions take place.
b. The adsorption phenomenon is assumed to occur at equilibrium with the reaction rate on the catalyst surface controlling the overall reaction.

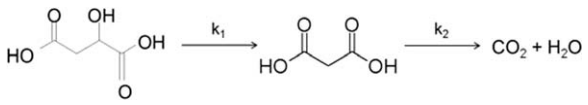

Figure 20. RN1–"Series" mechanism for the photocatalytic degradation of malic acid.

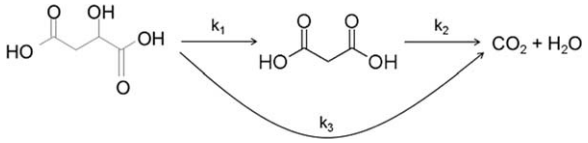

Figure 21. RN2–"In Series-parallel" mechanism for the photocatalytic degradation of malic acid.

Table 4. Kinetic Parameters for the Photoconversion of Malic Acid for the RN1 Model

Parameter	Value	95% CI
$k_1(\text{min}^{-1})$	1.082×10^{-2}	1.680×10^{-3}
$k_2(\text{min}^{-1})$	3.047×10^{-3}	4.442×10^{-4}
K^A_{MaAc} (ppm^{-1})	1.043×10^{-1}	2.220×10^{-2}
$K^A_{\text{MAc}}(\text{ppm}^{-1})$	2.859×10^{-3}	6.064×10^{-4}

Initial malic acid concentrations:10, 20, 30, and 40 ppm. DOF:380.

c. The final CO_2 and H_2O products formed at the end of the reaction do not adsorb on the catalyst surface.
d. The photolysis of malic acid and malonic acid is considered negligible.

In the case of this study, given the asymmetrical radiation profile caused by the position of the lamp in the setup, and the poorly irradiated regions close to the edges of the CREC-photoreactor cell, the photoconversion rate has to consider a local volumetric rate of photon absorption (LVRPA) as suggested by Toepfer et al.[44]

$$-r_i = k_{T,i}(\text{LVRPA})^m \frac{K^A_i C_i}{1+\sum_{j=1}^{n} K^A_j C_j} = \frac{k^k_i K^A_i C_i}{1+\sum_{j=1}^{n} K^A_j C_j} \quad (6)$$

where i represents the main species being degraded, "j" denotes each component that appears in the reaction, n is the number of species participating in the reaction, r_i is the reaction rate (mol $g^{-1}_{\text{catalyst}}\text{h}^{-1}$), $k_{T,i}$ denotes the kinetic constant independent of photon absorption, LVRPA stands for the local volumetric rate of photon absorption (W m^{-3}), m represents the order of reaction related to LVRPA ($0.5 < m < 1$), K^k_i denotes the reaction kinetic constant (mol $g_{\text{cat}}{}^{-1}$ h^{-1}), K^A_i stands for the adsorption constant (mol^{-1} l), and C_i represents the species' concentration (mol L^{-1}). In this equation, the terms LVRPA and m were constant in all the experimental runs.

In a photocatalytic reactor operating in a batch mode, similar to the photoreactor used in this research, the rate equation for the photoconversion of the "i" species can be expressed as[2]

$$-r_i = \frac{1}{W_{\text{irrad}}}\frac{dN_i}{dt} = \frac{V}{W_{\text{irrad}}}\frac{dC_i}{dt} \quad (7)$$

where W_{irrad} is the mass of TiO_2 in the catalyst film (g_{cat}), V is the reactor volume (L), N_{i} is the number of moles to be degraded (mol), and t is the reaction time (hour).

Combining the Eqs. 6 and 7, the reaction rate for each chemical compound can be written as

$$\frac{dC_i}{dt} = \frac{K_i C_i}{1+\sum_{j=1}^{n} K^A_j C_j} \quad (8)$$

where $k_1 = \frac{W_{\text{irrad}}}{v} k^k_i K^A_i$

On the basis of Eq. 8 and according to RN1 and RN2, the following set of differential equations are obtained. In the case of RN1 (refer to Figure 20)

$$\frac{dC_{\text{McAc}}}{dt} = \frac{-k_1 C_{\text{MaAc}}}{1+K^A_{\text{MaAc}}C_{\text{MaAc}}+K^A_{\text{MAc}}C_{\text{MAc}}} \quad (9)$$

$$\frac{dC_{\text{MAc}}}{dt} = \frac{k_1 C_{\text{MaAc}} - k_2 C_{\text{MAc}}}{1+K^A_{\text{MaAc}}C_{\text{MaAc}}+K^A_{\text{MAc}}C_{\text{MAc}}} \quad (10)$$

where MaAc and MAc refers to malic and malonic acid, respectively.

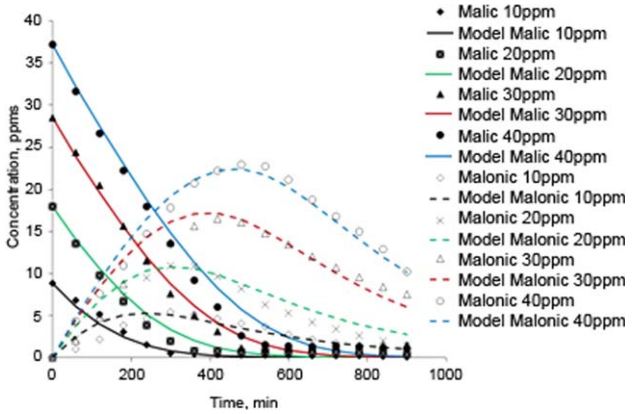

Figure 22. Experimental and RN1 model concentration profiles for malic acid and malonic acid during photocatalytic conversion using a TiO_2-film.

Initial concentrations: 10, 20, 30, and 40 ppm. [Color figure can be viewed in the online issue, which is available at wileyonlinelibrary.com.]

Conversely and given RN2 (see Figure 21), an alternate set of ordinary differential equations given by Eqs. 11 and 12 can be considered

$$\frac{dC_{\text{McAc}}}{dt} = \frac{-(k_1+k_3)C_{\text{MaAc}}}{1+K^A_{\text{MaAc}}C_{\text{MaAc}}+K^A_{\text{MAc}}C_{\text{MAc}}} \quad (11)$$

$$\frac{dC_{\text{MAc}}}{dt} = \frac{k_1 C_{\text{MaAc}} - k_2 C_{\text{MAc}}}{1+K^A_{\text{MaAc}}C_{\text{MaAc}}+K^A_{\text{MAc}}C_{\text{MAc}}} \quad (12)$$

Kinetic parameters for both RNs (RN1 and RN2) were calculated using the least squares fit as provided in MATLAB. The optimization of kinetic and adsorption parameters for malic and malonic acid degradation following RN1 are reported in Table 4. Model predictions compared with experimental results are presented in Figure 22 for different initial concentrations in the case of RN1. It can be concluded that the model obtained with the mechanism "in series" fits the experimental data very well yielding a R^2 of 0.983.

Values of the kinetic and adsorption constants for the RN1 are reported in Table 4. Calculations were performed with a degree-of-freedom (DOF) of 380. According to the relatively small values of the 95% confidence interval (CI), it can be concluded that the kinetic model proposed, predicts the data obtained very well.

Table 5 reports the cross-correlation coefficients for different parameters obtained in the modeling when an "in series" kinetic model is used (RN1). Considering the values reported in this table, it is observed that all parameters display cross-correlation coefficients much smaller than 1 with the only exception of k_1 and K^A_{MaAc} with a 0.93 coefficient. This behavior is expected given the nature of the L–H model, where kinetic and adsorption constants are present in both the numerator and denominator of the rate equations.[27–29,38]

Figure 23 reports the experimental and estimated photocatalytic degradation profiles of malic and malonic acid using the RN2. Results are reported for initial concentrations of malic acid, with these being 10, 20, 30, and 40 ppm. This model also shows a very good fit between the experimental and model concentration profiles for malic and malonic acid photodegradation yielding a R^2 of 0.988.

Table 5. Cross-Correlation Coefficients of the Kinetic and Adsorption Parameters for the RN1 Model

Parameter	k_1	k_2	K^{A}_{MaAc}	K^{A}_{MAc}
k_1	1			
k_2	0.78	1		
K^{A}_{MaAc}	0.93	0.62	1	
K^{A}_{MAc}	0.58	0.86	0.30	1

Initial malic acid concentrations:10, 20, 30, and 40 ppm.

Table 6. Kinetic Parameters for the Photoconversion of Malic Acid Using RN2

Parameter	Value	95% CI
$k_1(min^{-1})$	1.365×10^{-2}	2.285×10^{-3}
$k_2(min^{-1})$	2.429×10^{-3}	3.977×10^{-4}
$k_3(min^{-1})$	2.942×10^{-3}	1.097×10^{-3}
K^{A}_{MaAc} (ppm^{-1})	1.758×10^{-1}	4.375×10^{-2}
K^{A}_{MAc} (ppm^{-1})	4.109×10^{-3}	6.203×10^{-4}

Initial concentrations: 10, 20, 30 and 40 ppm. DOF: 379

Table 6 gives the values for the kinetic and adsorption constants involved in the "in series-parallel" kinetic model (RN2). The DOF in this calculation is 379. This table also shows the 95% CI as well as the standard deviation values. This second model also presents narrow spans for both the CI and STD. Therefore, the proposed mechanism from the photocatalytic degradation experiments can be considered to predict the experimental data well.

Table 7 reports the cross-correlation coefficients for different parameters obtained with the RN2 "in series-parallel" model. With respect to the cross-correlation coefficients determined, one can see that k_1 and K^{A}_{MaAc} display a cross correlation coefficient of 0.98 while k_3 and K^{A}_{MaAc} have a value of 0.90. Thus, while one may gain a better experimental data description with RN2, there is increased uncertainty on the actual values of some of the kinetic constants determined with this reaction network.

Furthermore, reconciliation plots provided a good understanding of the reliability of the parameters obtained. It is known that plots presenting vertical bands show an overparameterization of the kinetic model. The presence of horizontal bands in the reconciliation plots may indicate that the model is somewhat incomplete with at least one parameter missing in the kinetic model. For both RNs, it was found that no horizontal or vertical lines were formed during the reconciliation plots (results not shown here). Therefore, it is concluded that for both RN1 and RN2, experimental and modeled points are randomly distributed.

Figure 24 reports the concentration profile of Carbon in ppm, for the CO_2 and the Total Organic Carbon (TOC) in experiments with an initial concentration of 40 ppm of malic acid. On this basis, it can be shown that carbon balances close at 2–3%. Furthermore, Figure 24 is valuable to further elucidate the adequacy of RN1 and RN2 kinetic models. One can see that there is CO_2 formation from the very beginning of the photocatalytic reaction. This shows that complete mineralization of malic acid fractions into CO_2 and H_2O takes place at the early stages of the photocatalytic conversion already.

However, one can also notice that the rate of CO_2 formation (in ppm of carbon) is smaller than the rate of malic acid photoconversion (about 1 mole of CO_2/2 moles of malic acid ratio). This shows that the RN2 or the "in series-parallel" model better predicts malic acid photocatalytic conversion. This higher reliability of the "in series-parallel" overall mechanism was also observed in the photocatalytic degradation of phenol in water using a cylindrical slurry unit.[27] According to this author, the "in series-parallel" mechanism dominates due to a nonuniform OH radical density in the Photo-CREC Water II unit.

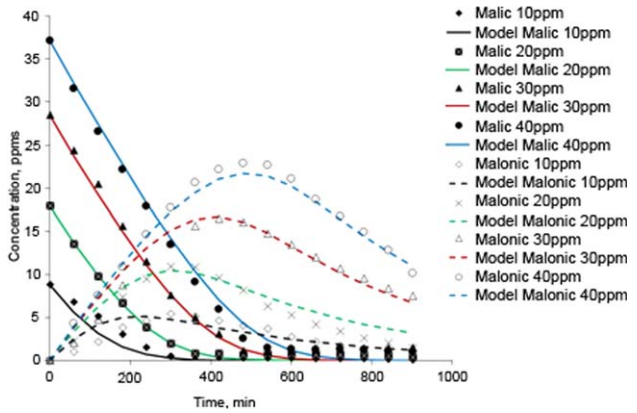

Figure 23. Experimental and RN2 (in series-parallel model) concentration profiles for malic acid and malonic acid during photocatalytic conversion in (on) TiO_2-films.

Initial concentrations: 10, 20, 30, and 40 ppm. [Color figure can be viewed in the online issue, which is available at wileyonlinelibrary.com.]

Quantum yield calculations

Values of quantum yields were determined by applying the minimum apparent quantum yield concept, which consists of the ratio between the numbers of molecules of the OH radicals converted per unit time to the number of photons absorbed by the catalyst film per unit time. This definition of quantum yield is described in the following equation

$$\varphi = \frac{\text{Number of molecules of OH}^{\cdot}\text{ consumed/s}}{\text{Number of photons absorbed by the TiO}_2\text{ layer/s}} = \frac{\varphi_1}{P_a(t)} \quad (13)$$

$P_a(t)$ was calculated using the irradiation profile measured for different concentrations of malic acid (10, 20, 30, and 40 ppm). The number of molecules of OH radicals consumed/s (φ_1) was estimated through the malic acid degradation stoichiometry, considering the two possible mechanisms proposed: the "in series" reaction network (RN1) and "in series-parallel" reaction network (RN2).

The methodology reported by Serrano et al.[26] was used to calculate the quantum yield for RN2. This methodology uses

Table 7. Cross-Correlation Coefficients of the Kinetic Parameters in(check) the Photoconversion of Malic Acid for RN2

Parameter	k_1	k_2	k_3	K^{A}_{MaAc}	K^{A}_{MAc}
k_1	1				
k_2	0.24	1			
k_3	0.88	0.18	1		
K^{A}_{MaAc}	0.98	0.22	0.90	1	
K^{A}_{MAc}	0.26	0.06	0.53	0.22	1

Initial concentrations: 10, 20, 30, and 40 ppm

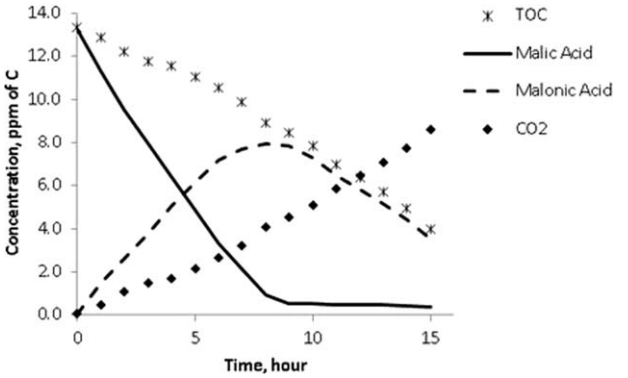

Figure 24. CO_2 and TOC profiles for the photocatalytic degradation of malic acid at an initial concentration of 40 ppm (13.6 ppm of carbon).

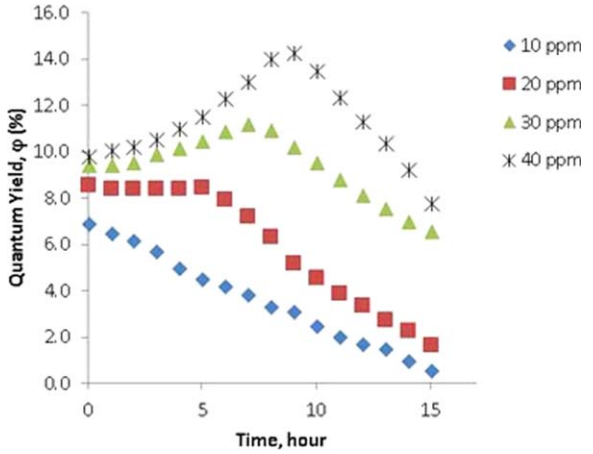

Figure 25. Quantum yields for malic acid photocatalytic degradation.

Initial concentrations: 10, 20, 30, and 40 ppm. kinetic reaction network: RN2. [Color figure can be viewed in the online issue, which is available at wileyonlinelibrary.com.]

the RN along with the stoichiometric amount of hydroxyl radicals required in each reaction step. For instance, for the RN2, malic acid degradation occurs with the consumption of four molecules of OH radicals in the first step. Consumption of eight molecules of hydroxyl radicals in the second step are required to form CO_2 and six H_2O molecules. This is described using the following equations

$$3C_4H_6O_5 + 4OH^{\cdot} \xrightarrow{k_1} 4C_3H_4O_4 + 3H_2O \quad (14)$$

$$C_3H_4O_4 + 8OH^{\cdot} \xrightarrow{k_2} CO_2 + 6H_2O \quad (15)$$

$$C_4H_6O_5 + 12OH^{\cdot} \xrightarrow{k_3} 4CO_2 + 9H_2O \quad (16)$$

In the RN2 mechanism for malic acid photoconversion, malic acid is converted into malonic acid. Malonic acid can be subsequently converted to CO_2. Conversely, malic acid can also be directly converted into CO_2, with water produced in the two pathways (refer to Figure 21).

Values of the quantum yields (φ) as a function of time for the photocatalytic conversion of malic acid at 10, 20, 30, and 40 ppm are shown in Figure 25. These results are presented for RN2. These outcomes illustrate that values of φ for the RN2, decrease with time, for the initial concentrations of 10 and 20 ppm of malic acid. This shows a maximum φ value in the very beginning of the reaction. For the other concentrations (30 and 40 ppm), φ increases in the beginning of the run until it reaches a maximum value coinciding with the maximum concentration of the intermediate formed (malonic acid), as observed when using RN2. The maximum value of φ is 14.2%, obtained after 9 h of photocatalytic conversion of malic acid at 40 ppm.

With quantum yield values as high as 14.2% (RN2), one can safely consider that the holes (h^+) formed in the quartz-glue-TiO_2 surface (back face) are mobile and that they can migrate to the opposite side of the TiO_2 layer in direct contact with the malic acid solution. This h^+ site mobility and migration promotes the formation of OH radicals which degrade the malic acid molecules.

As a result, and according to the information presented in the literature section, the required time for holes and electrons to reach the 1.3×10^{-6} m agglomerate surface as in the present study, is significantly 1.3×10^{-10} and 6.5×10^{-10} s, respectively. This is significantly smaller than the 8.9×10^{-5} s expected charges lifetime as quoted by Wilke and Breuer (1999). In summary, using the available literature data, one can justify the findings observed in the Photo-CREC cell: (a) charge carriers generated on the irradiated side of TiO_2 agglomerates have enough time to travel to the nonirradiated dark side of the TiO_2 agglomerates and (b) transported charge carriers have ample opportunity to react with the available organic chemical species in water.

When comparing the maximum value of quantum yields (singular or plural) obtained for the photocatalytic conversion of malic acid at 20 ppm initial concentration ($\varphi_{\text{series-parallel}} = 8.6\%$) with the best values reported in the literature being 6% φ,[13] it can be concluded that the CREC-photoreactor Cell with only "dark surfaces" contributing to photoactivity shows excellent performance. These data also highlight the importance of this article to clarify photoactivity of catalyst surfaces "non-directly" irradiated.

Conclusions

a. Photodegradation of organic species using a CREC-photoreactor cell with a thin TiO_2-film allows one to confirm the critical role of mobile electron holes on semiconductor surfaces in photocatalysis.
b. Macroscopic Radiation Balance measurements demonstrate that 92% of the light emitted is absorbed by the prepared TiO_2-film.
c. SEM/EDX spectroscopy analysis of the prepared thin TiO_2-film shows a wavy layer with two characteristic regions with different loading of TiO_2 particles.
d. Malic acid photoconversion allows one to demonstrate that Langmuir–Hinshelwood kinetics in conjunction with adequate reaction pathways such as the "in series-parallel" (RN2) network are required for photocatalytic kinetic modeling.
e. Both RN1 (in series network) and RN2 (in series-parallel network) provide a good fit of the experimental data with narrow spans. RN2 provides however, a better description of the CO_2 formed.
f. Quantum yields (φ) as high as 14.2% for a 40 ppm initial malic acid concentration using RN2 were obtained. This

confirms the role of "h^+ electron" mobile holes in "non-directly" irradiated thin TiO_2-films.

Acknowledgments

We express our appreciation to the Natural Sciences and Engineering Research Council of Canada for the financial support of this investigation. Authors would like to acknowledge Ms. F. de Lasa for her assistance on the preparation of this article.

Notation

C = Speed of light, m/s
C_i = "Species" concentration of component i, ppm
h = Planck's constant, J s
k_I = Apparent photocatalytic kinetic constant, min^{-1}
k_i^A = Adsorption constant, mol^{-1} l
k_i^k = Reaction kinetic constant, mol g_{cat}^{-1} h^{-1}
k_i = Apparent kinetic constant for species i, min^{-1}
k_m = Mass-Transfer coefficient, m/s
$k_{photolysis}$ = Kinetic constant for photolysis, min^{-1}
P_a = Rate of radiation absorbed, Photons/s
P_{bs} = Rate of radiation back scattered, Photons/s
P_l = Rate of radiation emitted, Photons/s
P_t = Rate of radiation transmitted, Photons/s
$q_{z,\lambda,t}$ = Radiative flux or Irradiation Intensity, $\mu W/cm^{2\alpha}$
r_i = Reaction rate of component i, mol $g_{catalyst}^{-1}$ h^{-1}
t = Reaction time, s
V = Reactor volume, L
W_{irrad} = Amount of TiO_2 catalyst irradiated, g
Wt % = Weight–weight percentage

Acronyms

BL = Black-light
CFR = Code of Federal Regulations
CFU = Colony-forming unit
CI = Confidence Interval
CREC = Chemical Reaction Engineering Centre
DOF = Degree-of-Freedom
FDA = Food and Drug Administration U.S.
HPLC = High-Performance Liquid Chromatograph
L–H = Langmuir–Hinshelwood
LVRPA = Local volumetric rate of photon adsorption, W/m^3
MaAc = Malic Acid
Mac = Malonic Acid
R^2 = Correlation Coefficient
RPM = Revolutions per minute
SEM = Scanning Electron Microscope
Sh = Sherwood number, dimensionless
STD = Standard Deviation
TOC = Total Organic Carbon
UV = Ultraviolet

Greek letters

φ_1 = Number of molecules of OH radical consumed/s, molecules/s
φ = Quantum Yield, %
λ = Wavelength, nm
α = Percentage of light accounted for Photolysis

Literature Cited

1. Herrmann J. Heterogeneous photocatalysis: fundamentals and applications to the removal of various types of aqueous pollutants. *Catal Today*. 1999;53:115–129.
2. de Lasa H, Serrano B, Salaices M. *Photocatalytic Reaction Engineering*. New York: Springer, 2005.
3. Enright B, Fitzmaurice D. Spectroscopic determination of electron and hole effective masses in a nanocrystalline semiconductor film. *J Phys Chem*. 1996;100:1027–1035.
4. Minder R, Ottaviani G, Canali C. Charge transport in layer semiconductors. *J Phys Chem Solids*. 1976;37:417–424.
5. Jacoboni C, Canali C, Ottaviani G, Alberigi Quaranta A. A review of some charge transport properties of silicon. *Solid State Electron*. 1977;20:77–89.
6. Wilke K, Breuer HD. The influence of transition metal doping on the physical and photo catalytic properties of titania. *J Photochem Photobiol A Chem*. 1999;121:49–53.
7. Tamaki T, Furube A, Murai M, Hara K, Katoha R, Tachiya M. Dynamics of efficient electron–hole separation in TiO_2 nanoparticles revealed by femtosecond transient absorption spectroscopy under the weak-excitation condition. *Phys Chem Chem Phys*. 2007;9:1453–1460.
8. Hanes DE, Worobo RW, Orlandi PA, Burr DH, Militotis MD, Robl MG, Bier JW, Arrowood MJ, Churev JJ. Inactivation of Crytosporidium parvum oocysts in fresh apple cider using ultraviolet irradiation. *Appl Environ Microbiol*. 2002;68:4168–4172.
9. Bolton JR, Linden KG. Standardization of methods for fluence UV dose determination in bench-scale UV experiments. *J Environ Eng*. 2003;29:209–215.
10. Duffy S, Churey J, Worobo R, Schaffner DW. Analysis and modeling of the variability associated with UV inactivation of Escherichia coli in apple cider. *J Food Prot*. 2000;63:1587–1590.
11. Basaran N, Quintero-Ramos A, Moake MM, Churrey JJ, Worobo RW. Influence of apple cultivars on inactivation of different strains of Escherichia coli O157:H7 in apple cider by UV irradiation. *Appl Environ Microbiol*. 2004;70:6061–6065.
12. Fernandez A, Lassaletta A, Jimenez VM, Justo A, Gonzalez-Elipe AR, Herman JM, Tahiri H, Ait-Ichou Y. Preparation and characterization of TiO_2 photocatalysts supported on various rigid supports (glass, quartz and stainless steel). Comparative studies of photocatalytic activity in water purification. *Appl Catal B*. 1995;7:49–63.
13. Danion A, Disdier J, Guillard C, Jaffrezic-Renault N. Malic acid photocatalytic degradation using a TiO_2-coated optical fiber reactor. *J Photochem Photobiol A*. 2007;190:135–140.
14. Sumin Z, Zaifeng S, Luyong W. Characteristics of TiO2 Film Immobilized on Glass and Stainless Steel Tube and Photodegradation of Phenol. In: International Conference on Computer Distributed Control and Intelligent Environmental Monitoring, Changsha, Hunan, China, February 19–20, 2011.
15. Choi H, Stathatos E, Dionysiou DD. Sol–gel preparation of mesoporous photocatalytic TiO_2 films and TiO_2/Al_2O_3 composite membranes for environmental applications. *Appl Catal B*. 2006;63:60–67.
16. Song YK, Park MK, Kwon YT, Lee HW, Chung WJ, Lee WI. Preparation of transparent particulate MoO_3/TiO_2 and WO_3/TiO_2 films and their photocatalytic properties. *Chem Mater*. 2001;13:2349–2355.
17. Herrmann JM, Tahiri H, Ait-Ichou Y, Lassaletta G, Gonzales-Elipe AR, Fernandez A. Characterization and photocatalytic activity in aqueous medium of TiO_2 and Ag-TiO_2 coatings on quartz. *Appl Catal B*. 1997;13:219–228.
18. Franch MI, Ayllon JA, Peral J, Domenech X. Fe III. *photocatalyzed degradation of low chain carboxylic acids implications of the iron salt*. *Appl Catal B*. 2004;50:89–99.
19. Rodgher V. *Photocalytic Degradation of Malic Acid Under Thin Coated TiO_2*. London, Ontario: The University of Western Ontario, 2012.
20. Bhatkhande DS, Pangarkar VG, Beenackers AACM. Photocatalytic degradation for environmental applications-A review. *J Chem Technol Biotechnol*. 2001;77:102–116.
21. Balasubramanian G, Dionysiou D, Suidan M, Baudin I, Laine JM. Evaluating the activities of immobilized TiO_2 powder films for the photocatalytic degradation of organic contaminants in water. *Appl Catal B*. 2003;47:73–84.
22. Gelover S, Gomez LA, Reyes K, Leal MT. A practical demonstration of water disinfection using TiO_2 fims and sunlight. *Water Res*. 2006;40:3274–3280.
23. Chen Q, Song JM, Pan F, Xia FL, Yuan JY. The kinetics of photocatalytic degradation of aliphatic carboxylic acids in an UV/TiO_2 suspension system. *Environ Technol*. 2009;30:1103–1109.
24. Irawaty W, Friedmann D, Scott J, Pichat P, Amal R. Photocatalysis and TiO_2 aqueous suspension: Effects of mono- or di-hydroxyl substitution of butanedioic acid on the disappearance and mineralisation rates. *Catal Today*. 2011;178:51–57.
25. Salaices-Arredondo M. *Photocatalysis in Slurry Reactors Radiation Transmission and Kinetic Modeling*. London, Ontario: The University of Western Ontario, 2002.

26. Serrano B, Ortız A, Moreira J, de Lasa H. Energy efficiency in photocatalytic reactors for the full span of reaction times. *Ind Eng Chem Res*. 2009;48:9864–9876.
27. Moreira del Rio J. *Photocatalytic Degradation of Phenolic Compounds in Water: Irradiation and Kinetic Modeling*. London, Ontario: The University of Western Ontario, 2011.
28. Moreira J, Serrano B, Ortiz A, de Lasa H. A unified kinetic model for phenol photocatalytic degradation over TiO_2 photocatalysts. *Chem Eng Sci*. 2012;78:186–203.
29. Moreira J, Serrano-Rosales B, Valades-Pelayo PJ, de Lasa H. Determination of kinetic parameter in a unified kinetic model for the photodegradation of phenol by using nonlinear regression and the genetic algorithm. *Int J Chem React Eng*. 2013;11:641–656.
30. Garcia Hernandez J, Serrano B, de Lasa H. The photocatalytic energy efficiency factors (PTEF) in photocatalytic reactors for air treatment. *Chem Eng J*. 2010;65:891–901.
31. de Lasa H, Serrano B, Salaices M. *Photocatalytic Reaction Engineering*. Springer, New York, 2005.
32. Irawaty W, Friedmann D, Scott J, Amal R. Relationship between mineralization kinetics and mechanistic pathway during malic acid photodegradation. *J Mol Catal A Chem*. 2011;335:151–157.
33. Mukherjee PS, Ray AK. Major challenges in the design of a large-scale photocatalytic reactor for water treatment. *Chem Eng Technol*. 1999;22:253–260.
34. Chen D, Li F, Ray AK. External and internal mass transfer effect on photocatalytic degradation. *Catal Today*. 2001;66:475–485.
35. Zepp RG, Cline DM. Rates of direct photolysis in aquatic environment. *Environ Sci Technol*. 1977;11:359–366.
36. Kormann C, Bahnemann DW, Hoffmann MR. Photolysis of chloroform and other organic molecules in aqueous TiO_2 suspensions. *Environ Sci Technol*. 1991;25:494–500.
37. Baxendale JH, Wilson JA. The photolysis of hydrogen peroxide at high light intensities. *Trans Faraday Soc*. 1957;53:344–356.
38. Ortiz-Gomez A, Serrano-Rosales B, Salaices M, de Lasa H. Photocatalytic oxidation of phenol: reaction network, kinetic modeling, and parameter estimation. *Ind Eng Chem Res*. 2007;46:7394–7409.
39. Moreira J, Serrano B, Ortiz A, de Lasa H. Evaluation of photon absorption in an aqueous TiO_2 slurry reactor using Monte Carlo simulations and Macroscopic Balance. *Ind Eng Chem Res*. 2010;49:10524–10534.
40. Moreira J, Serrano B, Ortiz A, de Lasa H. TiO_2 absorption and scattering coefficients using Monte Carlo method and macroscopic balances in a photo-CREC unit. *Chem Eng Sci*. 2011;66:5813–5821.
41. Salaices M, Serrano B, de Lasa HI. Photocatalytic conversion of phenolic compounds in slurry reactors. *Chem Eng Sci*. 2004;59:3–15.
42. Laoufi NA, Tassalit D, Bentahar F. The degradation of phenol in water solution by TiO_2 photocatalysis in a helical reactor. *Global NEST J*. 2008;10:404–418.
43. Montoya JF, Velasquez JA, Salvador P. The direct–indirect kinetic model in photocatalysis: a reanalysis of phenol and formic acid degradation rate dependence on photon flow and concentration in TiO_2 aqueous dispersions. *Appl Catal B*. 2009;88:50–58.
44. Toepfer B, Gora A, Gianluca LP. Photocatalytic oxidation of multicomponent solutions of herbicides: Reaction kinetics analysis with explicit photon absorption effects. *Appl Catal B*. 2006;68:171–180.

Manuscript received Sep. 20, 2013, and revision received Feb. 18, 2014.